Scanning Microscopy

Volume 6 | Number 4 Article 6

10-18-1992

The Spatial Distribution of Backscattered Electrons Revisited with a New Monte Carlo Simulation

Kenji Murata
University of Osaka Prefecture

Masaaki Yasuda
University of Osaka Prefecture

Hiroaki Kawata
University of Osaka Prefecture

Scanning Microscopy, Vol. 6, No. 4, 1992 (Pages 943-954)
Scanning Microscopy International, Chicago (AMF O'Hare), IL 60666 USA

0891-7035/92$5.00+.00

THE SPATIAL DISTRIBUTION OF BACKSCATTERED ELECTRONS REVISITED WITH A NEW MONTE CARLO SIMULATION

Kenji Murata*, Masaaki Yasuda and Hiroaki Kawata

Department of Electronics, College of Engineering
University of Osaka Prefecture
Sakai, Osaka 593, Japan

(Received for publication May 5, 1992 and in revised form October 18, 1992)

Abstract

A Monte Carlo simulation program including the discrete energy loss process has been developed, based on the Mott cross section for elastic scattering and the Vriens cross section for inelastic scattering. A deficiency of the previous model which is based on the screened Rutherford cross section and the Bethe law is made clear, from comparison between the new and old results such as the energy distribution of backscattered electrons for a Cu target. With the new Monte Carlo model, the radial spreading and penetration depth of both all and low-loss backscattered electrons have been studied for the Cu target at electron energies of 5, 10 and 20 keV. From these studies, it is found that the electron exit angle dependence of the spatial spreading is more significant with the low-loss backscattered electrons and a very high resolution of 2 to 3 nm can be obtained even with backscattered electrons.

Key Words: Monte Carlo simulation, backscattered electron, spatial distribution, discrete energy loss process.

*Address for correspondence
Kenji Murata
Department of Electronics,
College of Engineering,
University of Osaka Prefecture
1-1 Gakuencho
Sakai, Osaka 593
Japan
Phone 0722-52-1161 ext. 2286
FAX 0722-59-3340

Introduction

When incident electrons penetrate into a target, they collide with atoms composing it, resulting in both direction change and energy loss, and some of them are backscattered from the target. The backscattering coefficient depends on the atomic number of the target more strongly than the secondary electron yield does. Because of these characteristics of the backscattered electrons (BSEs), they are often used to obtain the BSE image in scanning electron microscopy (SEM) and to detect registration marks in electron beam lithography. A great deal of study on BSEs have been done by many authors from various points of view.

At the 1973 SEM meeting one of the authors (K.M.) presented the spatial distribution of BSEs for a copper target (Murata, 1973), which was obtained by a Monte Carlo (MC) simulation based on both the screened Rutherford (ScR) cross section for elastic scattering and the continuous slowing-down approximation (CSDA) of Bethe for energy loss. However, the ScR cross section is not accurate because it is based on the Born approximation and the Bethe law neglects the energy straggling of incident electrons.

The present paper revisits the spatial distribution of BSEs with a new MC simulation which is based on Mott cross section for elastic scattering and the discrete energy loss process through use of the Vriens cross section (Vriens, 1966b) for inelasic scattering. Some results are compared with old MC results. All results are for Cu at normal incidence.

Theory

Prior to description of a new MC simulation model, basic equations for elastic and inelastic scattering are explained.

Elastic scattering cross section.

Previous MC results (Murata, 1973, 1974, 1976a, b) are obtained by using the ScR cross section which is derived on the basis of the

List of Symbols

$[dE/ds]_{Bethe}$	Bethe energy loss equation
$[dE/ds]_{cont}$	Continuous energy loss rate
$[dE/ds]_{dis}$	Energy loss rate due to inelastic collisions
$[dE/ds]_{free}$	Energy loss rate due to free electron excitations
$[dE/ds]_{ion}$	Energy loss rate due to ionizations
$[dE/ds]_{JL}$	Energy loss equation of Joy & Luo
$[d\sigma/d\varepsilon]_{M}$	Møller cross section
$d\sigma_i/d\varepsilon$	Inelastic differential cross section of an i-th shell electron
$[d\sigma/d\Omega]_{Mott}$	Elastic scattering cross section of Mott
$d\eta/dw$	Energy distribution of backscattered electrons (BSEs)
E	Primary electron energy
E_0	Incident electron energy
e	Electron charge
$F(r)$	Integrated function of $f(r)$
$f(r)$	Radial distribution of BSEs
J	Mean ionization potential in the Bethe equation
N	The number of atoms per unit volume
$n(z)$	Distribution of the maximum penetration depth of BSEs
R	Electron range
R_∞	Rydberg constant
r	Radial distance
URN	Uniform random number
U_i	Binding energy of an i-th shell electron normalized by E
w	E/E_0
Z	Atomic number
Z_f	The number of free electrons
Z_i	The number of i-th shell electrons
z	Depth
$\bar{z}$	Mean depth of BSEs
z_{max}	Maximum penetration depth of BSEs
ΔE	Incremental energy loss
ΔE_c	Lower limit of energy transfer to free electrons
Δs_i	Free path length of an electron
η	Backscattering coefficient
ε	Transferred energy normalized by E
ε_c	$\Delta E_c/E$
σ_i	Inelastic cross section of an i-th shell electron
σ^{el}	Total elastic cross section per unit volume
σ^{in}	Total inelastic cross section per unit volume
σ_f	Inelastic cross section of a free electron-electron collision
σ_{tot}	Total cross section of elastic and inelastic collisions per unit volume
θ_p	Scattering angle of the primary electron when an inelastic collision occurred
θ_s	Scattering angle of the secondary electron when an inelastic collision occurred
ϕ	The exiting angle of BSEs

Note that all equations are expressed in cgs•esu units.

Born approximation. The Mott cross section is more accurate because it is the exact solution of the Dirac relativistic wave equation based on the partial wave expansion method. Examples of the Mott cross section normalized by the ScR cross section where the screening parameter by Nigam et al. (1959) is used are shown in Fig.1 in a polar diagram for Cu (Kotera et al.,1981,Kotera,1989). The Hartree-Fock atomic potential is used for calculations of Mott cross sections. If the curve is a circle with a radius of unity,both cross sections coincide with each other. As seen in Fig.1,even the curve for 20 keV deviates from the circle. The lower the incident electron energy is,the larger the deviation is. The Mott cross sections are larger than the ScR cross sections in medium to high scattering angles,resulting in larger probability in the backward scattering.

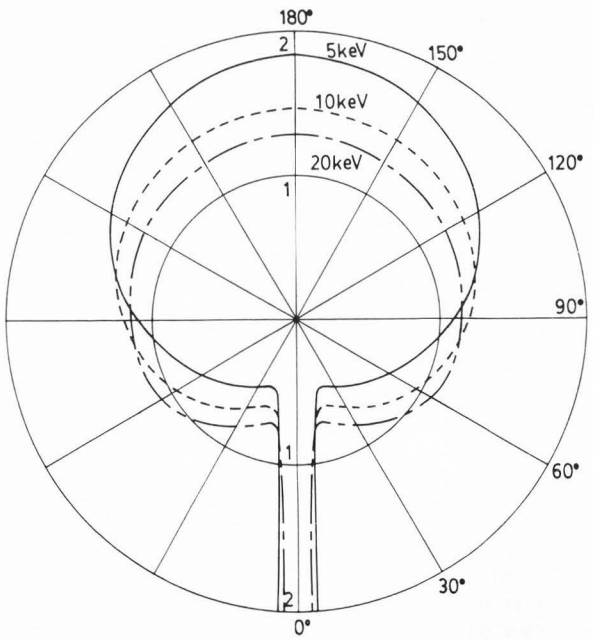

Fig.1. $[d\sigma/d\Omega]_{Mott}/[d\sigma/d\Omega]_{ScR}$ as a function of scattering angle at 5,10 and 20 keV. The value of 0° corresponds to the forward scattering.

Inelastic scattering cross section.

Murata et al. (1981) have published a MC model of fast secondary electron production by using the Møller equation for inelastic scattering (Møller, 1931). The equation for nonrelativistic electrons is given by:

$$\left[\frac{d\sigma}{d\varepsilon}\right]_M = \frac{\pi e^4}{E^2}\left\{\frac{1}{\varepsilon^2}+\frac{1}{(1-\varepsilon)^2}-\frac{1}{\varepsilon(1-\varepsilon)}\right\}, \quad (1)$$

where e is electron charge, E the primary electron energy and ε the transferred energy normalized by E. Since the cross section assumes free electrons for all atomic electrons, this is not appropriate especially for high atomic number elements. Later, Pandey and Rustgi (1989) proposed a model taking into consideration the bound electrons by limiting the application range of the cross section to electron energies above the binding energy and also showed that the energy, angular distribution and coefficients of transmitted and backscattered electrons in Al films calculated with this model were similar to those obtained with the Gryzinski cross section (Gryzinski, 1965).

Vriens (1966b) has derived the following quantum mechanical differential cross section for unpolarized beam-atom collisions.

$$\frac{d\sigma_i}{d\varepsilon} = \frac{\pi e^4}{E^2(1+2U_i)}\left[\left\{\frac{1}{\varepsilon^2}+\frac{4U_i}{3\varepsilon^3}\right\}+\left\{\frac{1}{(1+U_i-\varepsilon)^2}+\frac{4U_i}{3(1+U_i-\varepsilon)^3}\right.\right.$$
$$\left.\left.-\frac{\Phi}{\varepsilon(1+U_i-\varepsilon)}\right]\right., \quad (2)$$
$$\Phi = \cos\left\{-\left(\frac{R_y}{1+U_i}\right)^{1/2}\ln U_i\right\},$$

where U_i is the binding energy of an i-th shell electron normalized by E, R_y is the Rydberg energy normalized by E and the equation should be applied to the energy range of $U_i < 1$. The first, second and third terms in the bracket are the direct, exchange and interference terms, respectively. Φ expresses the cosine of the phase difference between direct and exchange scattering waves. For large E the value of Φ is approximated by 1. This equation reduces to a nonrelativistic form of the Møller equation when $U_i = 0$, assuming $\Phi = 1$. Proykova (1980) has performed MC simulation by using the old cross section by Vriens (1966a), which does not include the second and third terms and the minor correction by Vriens (1966b). Kolbenstvedt (1967) has derived the cross section for electron-electron scattering both in motion from the relativistic quantum theory, and has shown that when one of the electrons before collision is at rest, this equation reduces to the Møller equation and to eq.(2) for nonrelativistic electrons.

In the present paper, we perform MC simulation based on the Vriens cross section (1966b), derived from the binary encounter theory, and check the applicability of the model to backscattering phenomena in SEM.

Vriens' total ionization cross section of an i-th shell electron is given by

$$\sigma_i = \int_{U_i}^{\frac{1+U_i}{2}} \frac{d\sigma_i}{d\varepsilon}\, d\varepsilon$$
$$= \frac{\pi e^4}{E^2(1+2U_i)}\left(\frac{5}{3U_i}-1-\frac{2}{3}U_i+\frac{\ln U_i}{1+U_i}\right). \quad (3)$$

Since we can not distinguish which electron is the primary electron after interaction, the integration is done in the range of $(U_i, 0.5(1+U_i))$.

Energy loss.

Since the lower limit of energy transfer to free electrons, $\Delta E_c/E = \varepsilon_c$, can not be zero and collective excitation of plasmons is not considered here, there still remains the continuous energy loss process. This energy loss rate will be obtained by subtracting the discrete energy loss rate $[dE/ds]_{dis}$ from the Bethe equation $[dE/ds]_{Bethe}$ as follows:

$$\left[\frac{dE}{ds}\right]_{cont} = \left[\frac{dE}{ds}\right]_{Bethe} - \left[\frac{dE}{ds}\right]_{dis}, \quad (4)$$

where $[dE/ds]_{dis}$ is the sum of $[dE/ds]_{ion}$ and $[dE/ds]_{free}$ which are the energy loss rates by ionization of shell electrons and by free interactions, respectively, in the following.

$$\left[\frac{dE}{ds}\right]_{dis} = \Sigma N Z_i \int_{U_i}^{\frac{1+U_i}{2}} E\varepsilon \frac{d\sigma_i}{d\varepsilon}\, d\varepsilon + N Z_f \int_{\varepsilon_c}^{\frac{1}{2}} E\varepsilon \left[\frac{d\sigma}{d\varepsilon}\right]_M d\varepsilon$$
$$= \frac{\pi e^4 N}{E}\left[\frac{Z_i}{1+2U_i}\left\{\frac{2}{3}-3\ln 2+\frac{1}{3}(1+U_i)(1-2U_i)+3\ln(1+U_i)\right.\right.$$
$$\left.\left.-\ln U_i\right\}+Z_f\left\{2-3\ln 2-\frac{1}{1-\varepsilon_c}-2\ln(1-\varepsilon_c)-\ln\varepsilon_c\right\}\right], \quad (5)$$

where N: the number of atoms per unit volume, Z_i : the number of i-th shell electrons, Z_f : the number of free electrons and the summation of the first term is done for shell electrons which have the value of U_i less than unity. The binding energies, the number of shell electrons (Liljequist, 1983) and the energy loss rate due to ionization of shell electrons at 20 keV are shown in Table 1. The average binding energy is used for L shell electrons. 3d electrons are assumed to be free electrons because of loose binding, so that there are $Z_f = 11$ free electrons.

Type	1	2	3	4	free	Elastic
Shell	1s	2s2p	3s	3p	3d4s	
E_b (keV)	8.98	0.977	0.12	0.074	− − −	
Z_i	2	8	2	6	11	
λ_i (μm)	372	3.31	1.36	0.276	0.0333	0.00625
$(dE/ds)_i$ (eV/nm)	0.016	0.415	0.279	0.741	1.98	

Table 1. The binding energies (E_b in keV) and the number of electrons the inelastic mean free path and the energy loss rate due to ionization of shell electrons at 20 keV for Cu. ΔE_c=10 eV.

Actually the following modified equation by Joy and Luo (1989) is used instead of the original Bethe equation.

$$\left[\frac{dE}{ds}\right]_{JL} = \frac{2\pi e^4 N}{E} Z \ln\left(1+\frac{1.166E}{J}\right), \quad (6)$$

where Z is the atomic number and J is the mean ionization potential.

Simulation model.

The basic idea of a MC simulation has been already reported in a previous paper (Murata and Kyser, 1987). A brief explanation of the present model is given here.

When an electron is incident on a target, the electron will have elastic or inelastic collisions at some depth as shown in Fig.2, depending on their cross sections, σ^{el} and σ^{in}, respectively. The values of σ^{el} and σ^{in} are calculated as follows:

$$\sigma^{el} = N\int [d\sigma/d\Omega]_{Mott} d\Omega, \quad (7)$$

$$\sigma^{in} = \Sigma N Z_i \sigma_i + N Z_f \sigma_f, \quad (8)$$

where σ_f is the total cross section for a free electron-electron collision and is given by:

$$\sigma_f = \int_{\varepsilon_c}^{\frac{1}{2}} \left[\frac{d\sigma}{d\varepsilon}\right]_M d\varepsilon = \frac{\pi e^4}{E^2}\left\{\frac{1}{\varepsilon_c} - \frac{1}{1-\varepsilon_c} + \ln\left(\frac{\varepsilon_c}{1-\varepsilon_c}\right)\right\}, \quad (9)$$

Putting $\sigma_{tot} = \sigma^{el} + \sigma^{in}$, a free path of the electron is given by:

$$\Delta s_i = -(\sigma_{tot})^{-1} \cdot \ln(URN), \quad (10)$$

where URN is a uniform random number. In Table 1 also the elastic and inelastic mean free paths are shown at 20 keV.

The probabilities of elastic and inelastic collisions are σ^{el}/σ_{tot} and σ^{in}/σ_{tot}, respectively. The determination of either elastic or inelastic scattering is done by allotting generated uniform random numbers, according to these probabilities.

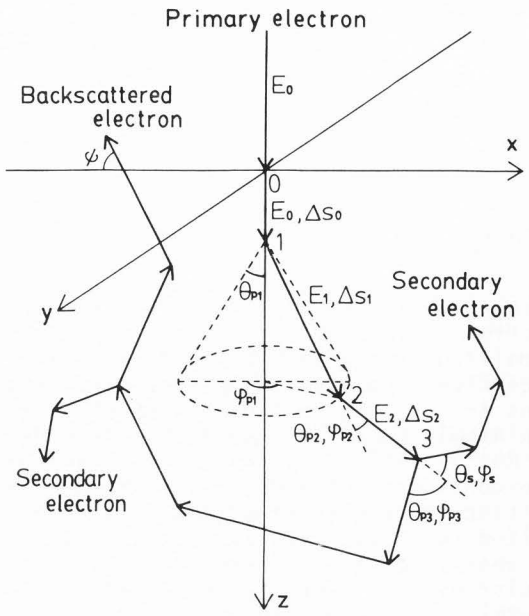

Fig.2. Electron trajectory model for a new Monte Carlo simulation.

When an elastic collision occurs, the angular deflection of the primary electron is calculated by using the Mott cross section. When an inelastic scattering occurs, the type of collision has to be determined, depending on the probabilities of σ_i/σ^{in} (i=1, 2, 3, 4) and σ_f/σ^{in}. The scattering angles θ_p and θ_s of the primary and secondary electrons, respectively, are given by, according to the momentum conservation rule.

$$\cos\theta_p = (1+1.5U_i-\varepsilon)/[(1+2U_i)\cdot(1+2U_i-\varepsilon)]^{1/2}, \quad (11)$$

$$\cos\theta_s = (\varepsilon+0.5U_i)/[(1+2U_i)\cdot(\varepsilon+U_i)]^{1/2}. \quad (12)$$

The continuous energy loss at a step with the length of Δs_i is calculated by:

$$\Delta E = |[dE/ds]_{cont}| \cdot \Delta s_i. \quad (13)$$

The electrons are tracked down to 500 eV. The numbers of simulated trajectories are 20,000, 20,000 and 10,000 for 5, 10 and 20 keV, respectively. For BSEs with low-loss energy less than ΔE 100,000 to 200,000 trajectories are simulated by limiting the energy of electrons to be traced to $E_0 - \Delta E$. The value of Berger-Seltzer (1964) is used for the mean ionization potential J in the modified Bethe equation. The value of ΔE_c is 10 eV.

Results and Discussions

Energy distribution of BSEs.

In Fig.3, the energy distributions of BSEs as a function of $w\ (=E/E_0)$ are compared between experimental (Kulenkampff and Spyra, 1954, Matsukawa et al., 1974, Darlington, 1975) and two MC results obtained with the new and old models. The distribution is known to be insensitive to the primary electron energy. The backscattering coefficients, η, of experiments of Kulenkampff & Spyra, Darlington, new and old MC simulations are 0.29, 0.309, 0.326±0.006 and 0.309±0.006, respectively. Although the absolute values of calculated $d\eta/dw$ are larger than the experimental value of Kulenkampff & Spyra owing to larger backscattering, both shape and peak energy of the new distribution agree well with the experimental ones, while the shape of the old distribution is not round and the peak energy shifts to a lower energy. The new result agrees well especially with the result of Darlington. This improvement is probably due to the scatter of electron energies with the discrete energy loss process incorporated. Similar results are obtained at incident energies of 5 and 10 keV.

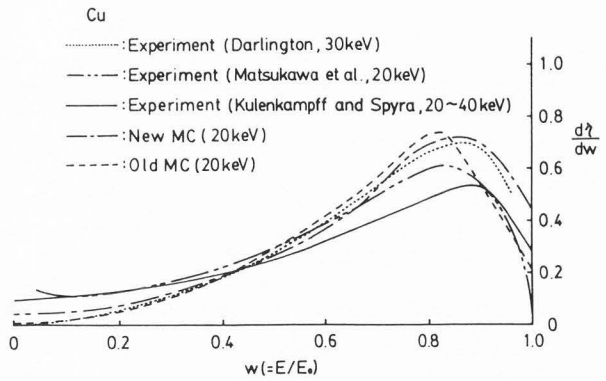

Fig.3. Energy distribution of backscattered electrons. Comparison is made among experimental (Kulenkampff & Spyra, 1954, Matsukawa et al., 1974, Darlington, 1975), new and old Monte Carlo results.

A more detailed comparison can be made for the energy distribution at a particular exit angle. In Fig.4 the two MC results of the energy distribution of BSEs are compared with experimental data obtained by Kulenkampff and Rüttiger (1954) at exit angles of 7°, 27° and 47° from the sample surface. The MC results are obtained by counting the numbers of electrons emerging in three different angle regions of 0°–20°, 20°–30° and 40°–50°, to reduce the statistical errors and dividing them by the solid angle in each angle region. The new results agree fairly well with the experimental in both shape and peak position although the MC results do not show a slow decrease with a decreasing energy. The old results show worse agreement with the experimental than the new results do, especially at the low exit angles of 7° and 27°. The calculated exit angle dependence of BSEs is confirmed to follow nearly a cosine law. A significant difference in the dependence is not seen between the new and old MC results.

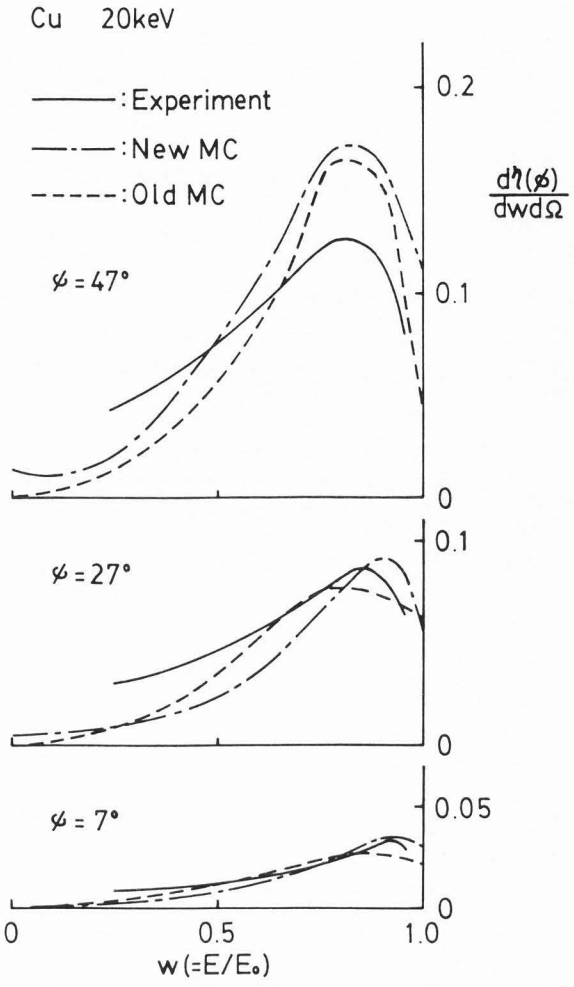

Fig.4. Energy distribution of backscattered electrons at exit angles of 7°, 27° and 47°. Comparison is made among experimental (Kulenkampff & Rüttiger, 1954), new and old Monte Carlo results.

Radial distribution of BSEs.

The calculated radial distributions, $f(r)$ (r is in μm unit), of BSEs at 20 keV are compared between the new and old models in Fig.5. The distributions are obtained by counting the number of BSEs emerging from the ring-shaped area between r and $r+\Delta r$, dividing it by the area element, $2\pi r\Delta r$, and by the number of incident electrons, and smoothing data points plotted at a radial distance

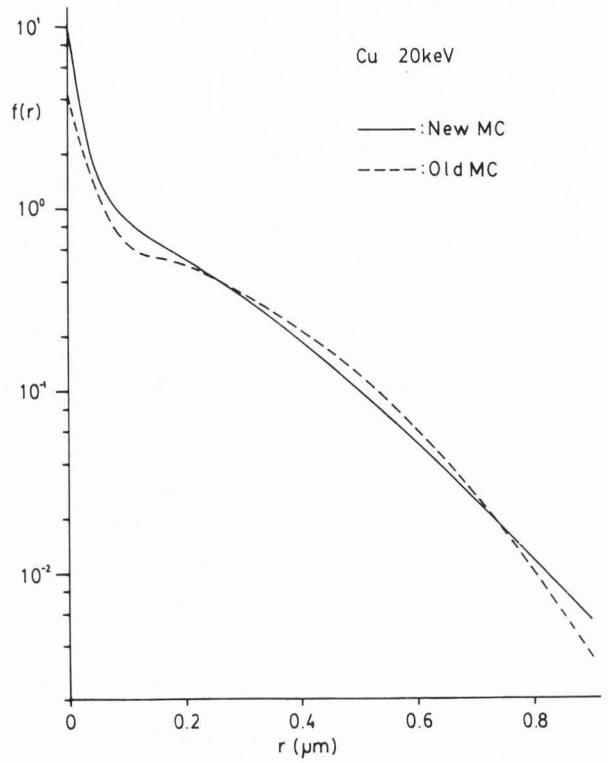

Fig.5.Radial distribution of backscattered electrons at 20 keV. Two Monte Carlo results are compared.

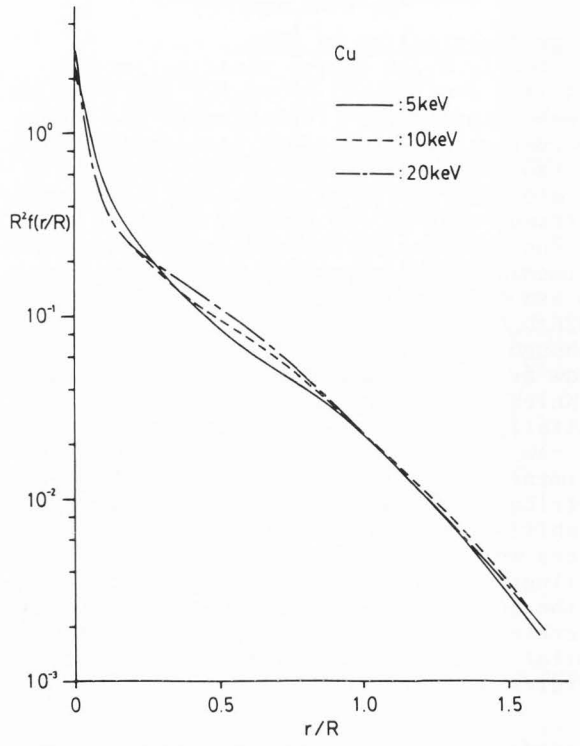

Fig.6.Normalized radial distribution of backscattered electrons at 5,10 and 20 keV.

of r+0.5Δr. As has been shown before (Murata, 1973,1974), the distributions have a sharp peak around the incident point and a broad background over the electron range. The new result has a higher peak and a more roundish change at the foot of the peak distribution than the old one does. As a contribution of single large angle BSEs to the peak seems to be large, the higher peak with the new model is probably caused by a larger backward scattering probability of the Mott cross section as seen in Fig.1. The roundish change is caused by the energy straggling effect.

Note that Nosker (1969) has reported a similar distribution based on the single large angle scattering model of Everhart (1960).

The new MC results of f(r) are compared in Fig.6 at various energies in a form normalized by R, the electron range, which is defined here. A method to obtain the value of R is the following. The integrated function of f(r), $F(r)=\int 2\pi f(r)\, rdr/\eta$, is plotted as a function of r. Then, F(r) gives the fraction of electrons which are backscattered within the radius of r. The range R is defined to be the radial distance where the tangential line at a linear part of the curve, F(r), crosses the line of F(r)=1.0. The range R will be the extrapolated electron range in the radial direction. The values of R are 0.050, 0.163 and 0.538 μm at 5, 10 and 20 keV, respectively. The ordinate is given by $R^2 f(r/R)$. The curves agree well with each other. This means that the electron diffusion is similar at any incident energies. An approximate distribution can be deduced at arbitrary energies in the energy range of 5 to 20 keV.

The exit angle dependence of the radial distribution was also investigated by dividing the exit angle ϕ into the three regions of 0°-30°, 30°-60° and 60°-90°. However, it was found that the distributions did not differ so much from each other and agreed with that for the total BSEs as shown in Fig.5 although a difference is seen in the intensity.

Radial distribution of low-loss BSEs.

As shown by Wells (1971,1972), the resolution of the BSE image can be improved by detecting low-loss BSEs because of their small diffusion range. Some evidence for this fact has been shown before (Murata, 1973). More details are given here. Typical results of the radial distribution of low-loss (ΔE≤1 keV) BSEs at 20 keV are shown in Fig.7, comparing between the new and old models. The cell size is 5 nm except near the incident point where the 1 nm cell is used. Both re-

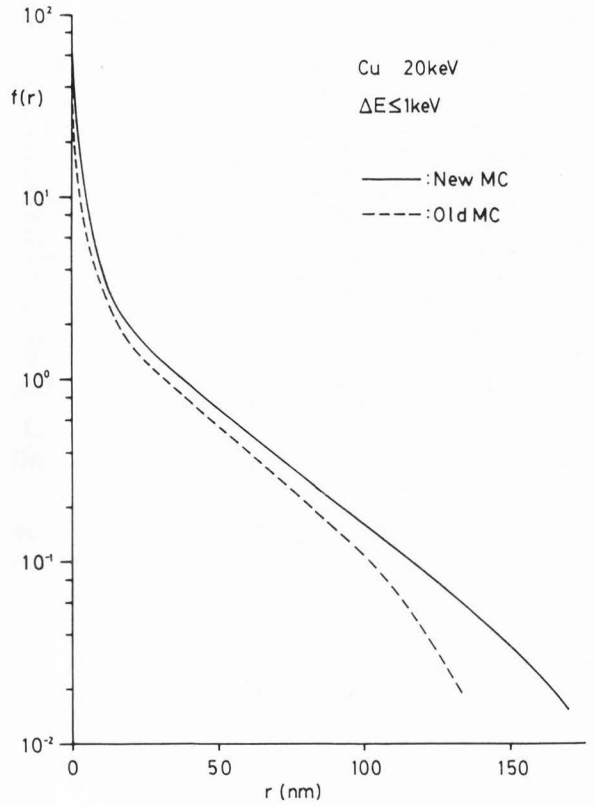

Fig.7.Radial distribution of low-loss (ΔE≤1keV) backscattered electrons at 20 keV.

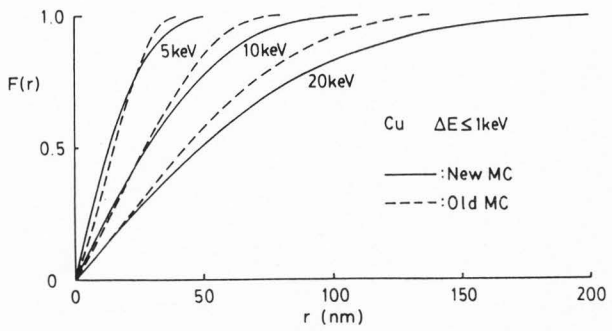

Fig.8.Fractional backscattering coefficients for low-loss backscattered electrons. The new and old Monte Carlo results are compared at 5,10 and 20 keV.

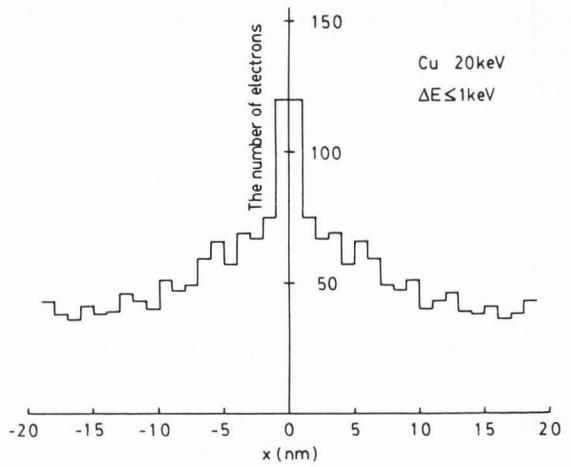

Fig.9.Lateral distribution of low-loss (ΔE≤1keV) backscattered electrons at 20 keV. The number of electrons are counted in a width of Δx=1 nm.

sults are very similar and show still the peak and background although the background is greatly reduced and its spreading is limited to the electron range to travel till electrons lose an energy less than 1 keV. The difference between the two models is only in the intensity. The old result does not show the shoulder at the foot of the peak distribution. This shows that the single large angle scattering is dominant and the energy straggling is not significant for low-loss BSEs. The calculated backscattering coefficients within radii of 5,25,50 and 100 nm with the new model are 0.0021,0.011 and 0.023 and 0.049 for the BSEs including all energy loss processes,and 0.0015,0.0066,0.013 and 0.020 for the low-loss BSEs,respectively. Their proportions are 71,59,55 and 41%,respectively. This means that the contribution of low-loss BSEs to the total backscattering is greater in more vicinity of the electron incident point. Therefore, it seems that the peak is built mainly by low-loss BSEs electrons,i.e. single large angle BSEs.

In Fig.8 the fractional backscattering coefficients,F(r), for low-loss (ΔE<1keV) BSEs are given at 5,10 and 20 keV,comparing between the new and old models. The curves with the old model reach the saturation earlier than those with the new model do because of a shorter electron range. Assuming the spatial resolution of low-loss BSEs to be the radius where the half intensity is included,the resolutions with the new model are 13,29 and 49 nm at 5,10 and 20 keV,respectively.

Ogura et al.(1990) and Franchi et al. (1990) have shown that GaAs/AlAs and GaAs/GaAlAs superlattice structures can be observed with a resolution of 2 to 3 nm by using the semiconductor detector,which is known to be more sensitive to higher energy electrons. Probably the BSE image contrast is obtained with a sharp peak around the center. To give the evidence for this fact,we have to make the cell size small,then need more trajectories. In the present study we have not done this calculation. However,since a fairly large fraction of BSEs around the center is caused by low-loss electrons,it will be worthwhile to investigate this effect with the spatial distribution of low-loss BSEs. In Fig.9 the lateral distribution of low-

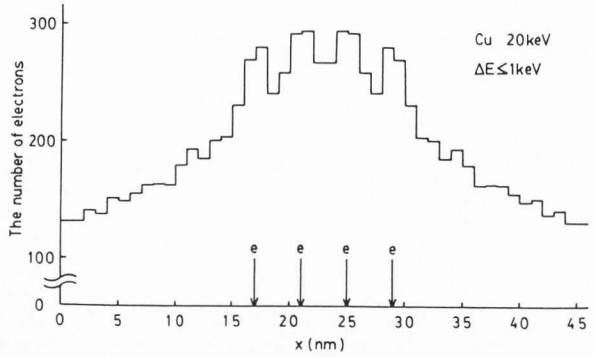

Fig.10. Lateral distribution of low-loss (ΔE≤1keV) backscattered electrons at 20 keV when four zero cross sectional electron beams are incident on a Cu target with the interval of 4 nm.

loss (ΔE≤1keV) BSEs at 20 keV is shown with the cell size of 1 nm when 100,000 electrons are incident at x=0 on a Cu target. The ordinate is the number of electrons counted in the area of (x,x+1nm). As seen in the figure, the peak is not lost although the background intensity is large due to the integration over one direction, y. Fig.10 is the lateral distribution of the low-loss BSEs when four electron beams are incident on the target with the interval of 4 nm. The result is not for the above superlattice structures, but it is important to know that the sharp peak keeps a spatial resolution of at least 2 nm. The peak intensity is determined by the atomic number of the sample around the incident point and the background intensity is determined by the average atomic number of the sample with fine structures regardless of the position of incidence. Therefore, it may be possible to obtain a sufficient contrast by the peak intensity with a high resolution if the background is subtracted in a some way. The peak/background ratio decreases with an increasing number of superposed distributions. In this case, the peak to background ratio is 0.91. A study of a resolution of BSEs with a single large angle scattering model will be an interesting future subject.

The exit angle dependence of the F(r) function of low-loss (ΔE≤250eV) BSEs is shown in Fig.11 at 20 keV, in comparison between the new and old models. A clear exit angle dependence is seen in the figure. The reason why this difference occurs can be explained in the following, assuming that the low-loss BSEs are caused by single large angle elastic scattering events. A trajectory model is shown in Fig.12 for this type of BSEs. The radial spreading of electrons exiting at an angle of ϕ from a depth z is $r=z\cdot\cot\phi$. The maximum value of r is given by the maximum penetration depth $z_{max}=\Delta s/(1+\mathrm{cosec}\phi)$, where $\Delta s=\Delta E/|[dE/ds]_{cont}|$ is the total travelling path

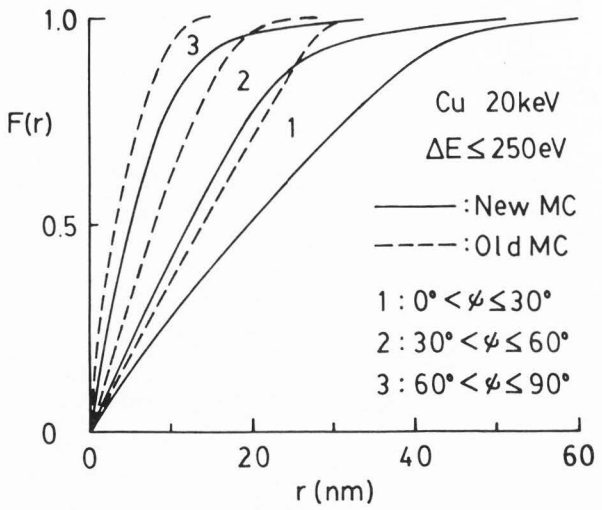

Fig.11. Exit angle dependence of F(r) of low-loss (ΔE≤0.25keV) backscattered electrons at 20 keV.

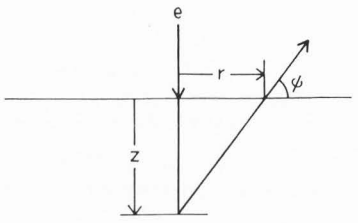

Fig.12. Trajectory model for a single large angle backscattered electrons.

length to lose an energy of ΔE=250eV, assuming that no discrete inelastic collisions occur. The values of r_{max} are 72, 42 and 19 nm in the exit angle regions of ϕ= 0°-30°, 30°-60° and 60°-90°, respectively. The calculated F(r) values saturate at about these maximum values. The old model predicts a faster saturation because of a shorter electron range. The radii including the half intensity with the new model are 19.5, 12.0 and 5.0 nm for the exit angle regions of 0°-30°, 30°-60° and 60°-90°, respectively. A resolution of 5.0 nm can be obtained at the highest exit angle region.

Maximum Penetration depth of BSEs.

It is often required to know the maximum penetration depth of BSEs in order to explain the BSE image in the SEM. Fig.13 shows the exit angle dependence of the maximum penetration depth distributions of all and low-loss (ΔE≤1keV) BSEs at 20 keV. The distributions for the all BSEs in the higher exit angle regions (30°-60° and 60°-90°) have a peak in deep depths. The reason why the peak is yielded is the following. The number

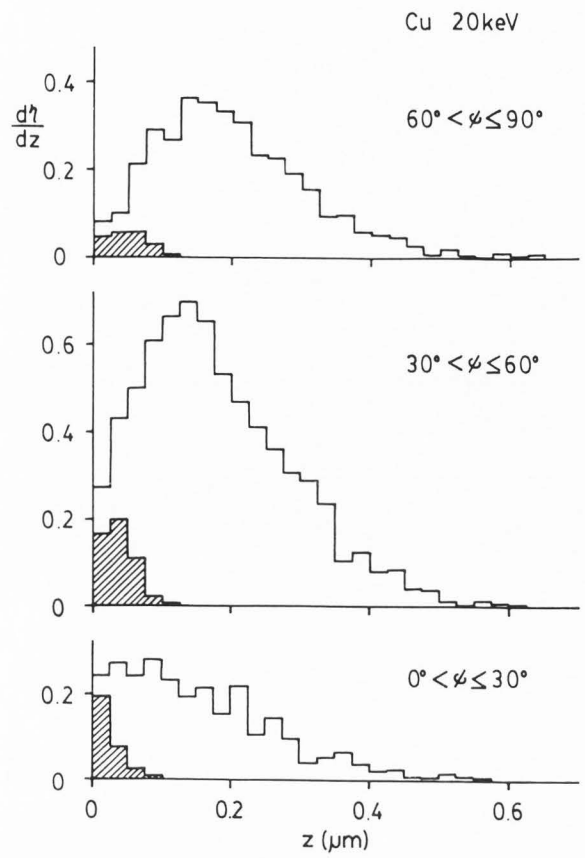

Fig.13. Maximum penetration depth distribution of the all and low-loss ($\Delta E \leq 1$keV, a shaded part) backscattered electrons in the three exit angle regions.

of BSEs increases with an increasing depth owing to single large angle backscattering events, plural and multiple scattering events, while the number of BSEs from deep depths decreases because such BSEs are easy to be deflected from the direction to the surface owing to a long travelling path length until they reach the surface. At shallow angles, the singly backscattered electrons do not increase so much with an increasing depth because the probability of being deflected by successive scattering events is high due to a long travelling path length to the surface as shown in Fig.12, consequently a significant peak can not be observed. In the low-loss curves the singly backscattered electrons are dominant very near the surface. The distribution is nearly flat over the depth of about 0.1 μm in the highest exit angle region of 60°-90°. This is caused mostly by single large angle BSEs. Namely, once they are scattered backward, they are easy to go out of the surface without any further scattering. In the lowest exit angle region the maximum penetration depth of electrons escaping from the sample will be smaller as explained in Fig.12.

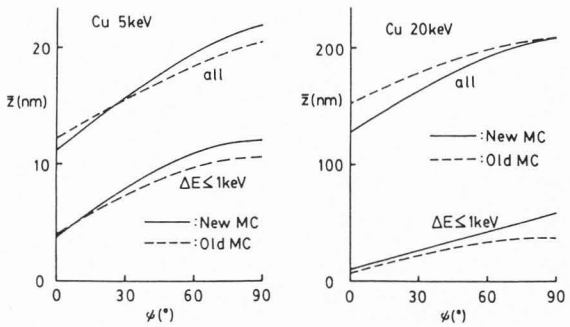

Fig.14. Exit angle dependence of the mean penetration depth of all and low-loss backscattered electrons at 5 and 20 keV. The new and old Monte Carlo results are compared.

Fig.14 shows the exit angle dependence of the mean penetration depth of the all and low-loss BSEs, which is calculated by $\bar{z}=\int n(z) \cdot z dz / \int n(z) dz$ where $n(z)$ is the number of electrons with penetration depth z, in comparison between the new and old models. Generally, the old model underestimates the mean penetration depth because of the neglect of the energy straggling effect. The low-loss BSEs have a stronger dependence than the total BSEs do. This is because the penetration depth of the low-loss BSEs is directly related to the value of z_{max} for the single large angle BSEs, which is proportional to $(1+\mathrm{cosec}\phi)^{1}$. The mean depths are about 10 and 60 nm at the lowest and highest angles, respectively. It should be noted that the radial spreading of the low-loss BSEs decreases with an increasing exit angle.

Conclusion

A new MC simulation model including the discrete energy loss process has been developed, based on the Mott cross section for elastic scattering and the Vriens cross section for inelastic scattering. The new results of the energy distribution of BSEs have shown better agreement with the experimental results than the old ones, which are obtained based on the ScR cross section and the Bethe law. We revisited the spatial distribution of BSEs for a Cu target with the new model. It is confirmed that the radial distribution has a peak and a broad background over the electron range. The introduction of the Mott cross section is found to give a higher peak intensity. This is favourable for high resolution observations with BSEs in SEM. Also the exit angle dependence of the spatial distribution of BSEs was studied with the new model and found to be significant for low-loss BSEs, to which a contribution of single large angle BSEs is dominant.

Applications of the new model to other elements such as Al and Au are in progress.

References

Berger MJ, Seltzer SM (1964)Tables of energy losses and ranges of electrons and positrons. Natl.Acad.Sci.Natl.Res.Council. Publ.1133,Washington D.C.,205-268

Darlington EH (1975)Backscattering of 10-100keV electrons from thick targets. J. Phys. D:Appl.Phys.8,85-93.

Everhart TE (1960)Simple Theory Concerning the Reflection of Electrons from Solids.J.Appl.Phys.31,1483-1490.

Franchi S,Merli PG,Migliori A,Ogura K, Ono A (1990)High-Resolution Backscattered Electron Imaging of GaAs/$Ga_{1-x}Al_xAs$ Superlattice Structures with a Scanning Electron Microscope. Proc.XIIth Int.Cong.for Electron Microscopy,San Francisco Press,San Francisco 380-381.

Gryzinski M (1965)Classical Theory of Atomic Collisions.I.Theory of Inelastic Collisions. Phys.Rev.138,A336-A358.

Joy DC,Luo Suichu (1989)An empirical stopping power expression for low energy electrons. Scanning 11,176-180.

Kolbenstvedt H (1967)Energy Transfer in the Collision of Electron Beams. Phys.Rev. 163,112-115.

Kotera M (1989)A Monte Carlo simulation of primary and secondary electron trajectories in a specimen. J.Appl.Phys.65,3991-3998.

Kotera M,Murata K,Nagami K (1981)Monte Carlo simulation of 1-10 keV electron scattering in a gold target. J.Appl.Phys.52,997-1003.

Kulenkapmff H,Rüttiger K (1954)Energie- und Winkelverteilung rückdiffundierter Elektronen. Z.Phys.137,426-434.

Kulenkapmff H,Spyra W (1954)Energieverteilung rückdiffundierter Elektronen. Z.Phys, 137,416-425.

Liljequist D (1983)A simple calculation of inelastic mean free path and stopping power for 50eV-50keV electrons in solids. J. Phys.D:Appl.Phys.16,1567-1582.

Matsukawa T,Shimizu R,Hashimoto H (1974) Measurements of the energy distribution of backscattered kilovolt electrons with a spherical retarding-field energy analyser. J. Appl.Phys.57,657-665.

Møller C (1931)Über den Stoß zweier Teilchen unter Berücksichtigung der Retardation der Kräfte. Z.Physik 70,786-795.

Murata K (1973)Monte Carlo Calculations on Electron Scattering and Secondary Electron Production in the SEM. Scanning Electron Microsc. 1973;II:267-276.

Murata K (1974)Spatial distribution of backscattered electrons in the scanning electron microscope and electron microprobe. J.Appl.Phys.45,4110-4117.

Murata K (1976a)Exit Angle Dependence of Penetration Depth of Backscattered Electrons in the Scanning Electron Microscope. phys.stat.sol.(a)36,197-208.

Murata K (1976b)Depth Resolution of the Low- and High-Deflection Backscattered Electron Images in the Scanning Electron Microscope. phys.stat.sol.(a)36,527-532.

Murata K,Kyser DF (1987)Monte Carlo Methods and Microlithography Simulation for Electron and X-ray Beams. Adv.Electro. and Elec. Phys.69,175-259.

Murata K,Kyser DF,Ting CH (1981)Monte Carlo simulation of fast secondary electron production in electron beam resists. J.Appl. Phys.52,4396-4405.

Nigam BD,Sundaresan BD,Wu T-Y (1959) Theory of multiple scattering:second Born approximation and correction to Moriere's work. Phys.Rev.115,491-502.

Nosker RW (1969)Scattering of Highly Focused Kilovolt Electron Beams by Solids. J. Appl.Phys.40,1872-1880.

Ogura K,Ono A,Franchi S,Merli PG, Migliori A (1990)Observation of GaAs/AlAs Superlattice Structures in both Secondary and Backscattered Electron Imaging Modes with an Ultrahigh Resolution Scanning Electron Microscope. Proc.XIIth Int.Cong.for Electron Microscopy,San Francisco Press,San Francisco 404-405.

Pandey LN,Rustgi ML (1989)A comparative study of electron transport phenomenon in the kev range. J.Appl.Phys.66,6059-6064.

Proykova A (1980)An analysis of scattering processes of conversion electrons in solid layers. J.Phys.D:Appl.Phys.13,291-305.

Vriens L (1966a)Binary-Encounter Electron-Atom Collision Theory. Phys.Rev.141,88-92.

Vriens L (1966b)Electron exchange in binary encounter collision theory. Proc.Phys. Soc.89,13-21.

Wells OC (1971)Low-Loss Image for Surface Scanning Electron Microscope. Appl.Phys. Letters 19,232-235.

Wells OC (1972)Explanation of the low-loss image in the SEM in terms of electron scattering theory. Scanning Electron Micorsc. 1972:169-176.

Discussions with Reviewers

D.Liljequist:Have you checked whether your correction term $[dE/ds]_{cont}$ in eq.(4) is always positive?

Authors:Let Z_s be the number of shell electrons which have the value of U_i less than unity,for example Z_s=8 and 18 for 0.5 and 20 keV,respectively. Assuming that these electrons have the smallest binding energy,i.e. 0.074 keV and U_i , $\varepsilon_c \ll 1$,eq.(5) reduces to

$$[dE/ds]_{dis} = (\pi e^4 N/E)\cdot\{Z_f(1-3\ln 2)-(Z_s \ln U_i + Z_f \ln \varepsilon_c)\}, \quad Z_f = Z_s + Z_f. \qquad (A)$$

This gives the largest value of $[dE/ds]_{dis}$. From eqs.(A),(5) and (6) the following condition for ε_c is deduced so that $[dE/ds]_{cont} > 0$.

$$E > 1.166^{-1} J \{(1.166/2)^a / U_i^{a-b} \varepsilon_c^{\,b} - 1\}, \qquad (B)$$

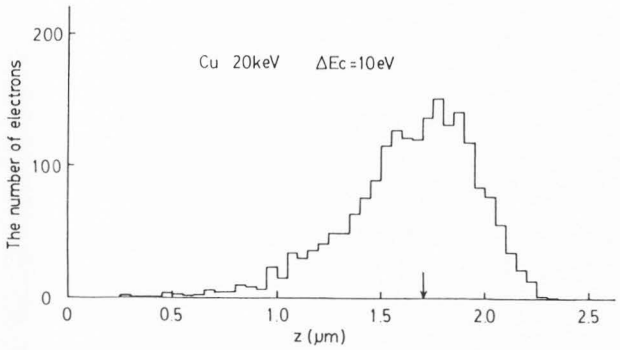

Fig 15 Distribution of electron stopping position in a Cu target at 20keV. 2000 electrons are incident. An arrow shows the Bethe range.

$a=Z_c/Z$, $b=Z_f/Z$.

If $a=1$ and $U_i=\varepsilon_c$, that is, all electrons are free, this condition is similar to the one proposed in a previous paper (K.Murata et al. (1981)) although an additional term 1.166^{1} is introduced, which comes from the use of the energy loss equation by Joy & Luo (1989). For $\Delta E_c=10$ eV this condition is sufficiently satisfied in the energy range of 0.5~20 keV.

D.Liljequist: Have you checked whether your choice of ΔE_c has any significant influence on your results?
G.Love: How is the lower limit of energy transfer to free electrons decided upon and is the MC model sensitive to the value selected?
R.Bindi: Have you tried to apply your model to describe the transmission of electrons through thin solid films?
Authors: First, we calculated the energy straggling of the primary electrons in a sample for $\Delta E_c=10, 20$ and 100 eV, assuming that the electrons penetrate straight without any angular deflection due to elastic and inelastic scattering events. An example of the distributions of electron stopping position in the sample is shown in the figure above. We could not see any significant difference among those results with $\Delta E_c=10, 20$ and 100eV.

Second, we calculated the energy distribution of transmitted electrons from thin films with various thicknesses for $\Delta E_c=10, 20$ and 100 eV. We confirmed that our results were not so sensitive to the selection of ΔE_c around 10 eV, but the result with $\Delta E_c=100$ eV showed a little higher peak intensity than those results with $\Delta E_c=10$ and 20 eV. Therefore, it is assumed that an appreciable decrease in the straggling effect will appear between 20 and 100 eV. However, comparisons with experimental data have shown a clear discrepancy in the peak intensity. Probably the model is still lack of the energy straggling.

R.Bindi: Could the authors comment the physical reason for the choice of low-loss energy, $\Delta E<1$keV or $\Delta E<250$eV?
Authors: The low-loss energy ΔE was set a few percent of the primary electron energy which has been used in the experiment of Wells (1971).

R.Bindi: What is the reason why you keep a continuous energy loss process in your model? Have you tried to apply an (experimental) dielectric loss function for the interactions with the jellium?
Authors: A decade ago we developed a Monte Carlo program which is based on the Møller cross section for free electron-electron collisions. The present model is just the extension of the previous model by replacing the Møller equation by the Vrien cross section and so the program was easily modified. Also the check of the validity of the Vriens equation for inelastic scattering is interesting. In addition, once this type of model is established, the model can be applied to any elements without special assumptions. The complete direct simulation which requires much computational time may not be necessary in applications to electron microprobe analysis.

We have not tried a dielectric loss function. It will be possible to combine the present model with the dielectric loss function. Since the experimental data for a Cu target are available (C.J.Powell, Electron Beam Interactions with Solids for Microscopy, Microanalysis and Microlithography, eds.D.F. Kyser, H.Niedrig, D.E.Newbury and R.Shimizu (SEM Inc., Chicago, 1984), p.19-31), it will be an interesting future subject.

Yen-Cai Ho: Would you assess the applicability of your model to heavy elements at low incident electron energies such as 1keV?
Authors: As previously reported (H.S.W.Massey and E.H.S.Burhop, Electronic and Ionic Impact Phenomena, vol.1 (Clarendon Press, Oxford, 1969), p.42) the Mott cross sections of Hg atoms are very accurate even at few hundreds eV. Therefore, the accuracy of the simulation for heavy elements and low incident electron energies depends mainly on the energy loss law of Joy and Luo (1989). Kotera et al. (1981) have shown that the calculated electron range and backscattering coefficient for a gold target through use of a Monte Carlo simulation based on the Mott cross section and the Rao-Sahib and Wittry equation agree well with the experimental ones even at 1keV. Further study is needed to see the applicability of the present model to various physical quantities under such conditions.

O.C.Wells: Cosslett published a paper in which BSE are subdivided between plurally scattered BSE and diffused BSE. I published a paper in which I tried to make this same distinction based on the observed energy

distribution of BSE for elements of different atomic number. Needless to say, the first of these emerged from a smaller area. Once again, I was wondering whether with the Monte Carlo method you might throw light on this question.

Authors: The author has discussed to some extent the effect of singly, plurally and diffused BSEs on the spatial distribution in a previous paper (K.Murata, 1973, 1974). However, the result is not satisfactory from a quantitative point of view. Fortunately, the Monte Carlo method can trace each electron and can make clear how many elastic scattering events each BSE suffers in a sample. We are planning to do it in the future.

J.Shou: How much does the applied "modified-Bethe" stopping power eq.(6) deviate from the "Standard stopping power" in ICRU Report 37?

Authors: Eq.(6) approaches a regular Bethe equation when E becomes large. The energy loss rates obtained from this equation are 13.0 and 7.71 MeV/(g/cm^2) at 10 and 20 keV, respectively (ρ=8.96 g/cm^3, J=322 eV) while the standard stopping powers are 13.2 and 8.07 MeV/(g/cm^2). At 20 keV there is a deviation of about 4% from the standard stopping power. Probably this deviation comes from the neglect of the relativistic effect. The introduction of the effect into the present model may improve the discrepancy in the backscattering coefficient.